



Experimental Heat Transfer

A Journal of Thermal Energy Generation, Transport, Storage, and Conversion

ISSN: 0891-6152 (Print) 1521-0480 (Online) Journal homepage: www.tandfonline.com/journals/ueht20


Experimental observations of the onset of unsteadiness for buoyant airflow along smooth and rough vertical isothermal walls

Giovanni Tanda, Essam Nabil Ahmed & Alessandro Bottaro

To cite this article: Giovanni Tanda, Essam Nabil Ahmed & Alessandro Bottaro (2025) Experimental observations of the onset of unsteadiness for buoyant airflow along smooth and rough vertical isothermal walls, *Experimental Heat Transfer*, 38:5, 505-517, DOI: [10.1080/08916152.2024.2357175](https://doi.org/10.1080/08916152.2024.2357175)


To link to this article: <https://doi.org/10.1080/08916152.2024.2357175>

 [View supplementary material](#) 

 Published online: 28 May 2024.

 [Submit your article to this journal](#) 

 Article views: 66

 [View related articles](#) 

 [View Crossmark data](#) 

 Citing articles: 1 [View citing articles](#) 

RESEARCH ARTICLE



Experimental observations of the onset of unsteadiness for buoyant airflow along smooth and rough vertical isothermal walls

Giovanni Tanda^a, Essam Nabil Ahmed^b, and Alessandro Bottaro^b

^aDIME, University of Genoa, Genoa, Italy; ^bDICCA, University of Genoa, Genoa, Italy

ABSTRACT

The buoyant airflow along a vertical isothermal wall, under conditions close to transitional, is studied. The schlieren technique and miniature thermocouples are employed for qualitative (flow unsteadiness) and quantitative (heat transfer coefficient and local air temperature) observations. For the smooth surface, the phenomena are found to be sensitive to the enclosure configuration surrounding the plate. Roughening the heated surface with staggered rib segments of proper dimensions leads to increased heat transfer, ascribed to the onset of unsteadiness close to the segments' edges, together with a better redistribution of the flow thanks to a favorable hydrodynamic interaction between fluid and protrusions.

ARTICLE HISTORY

Received 23 March 2023

Accepted 1 May 2024


KEYWORDS

Natural convection; transition; isothermal vertical plate; ribbed surface; schlieren

Introduction and literature review

Transition phenomena in natural convective boundary layers have been studied extensively from the past century to today. Linear stability theory as well as numerical calculations of the growth and non-linear interaction of two-dimensional and transverse disturbances have been applied to study initial instability for a variety of natural convection flows and conditions [1–3]. Dring and Gebhart [1] showed that as a disturbance in the flow adjacent to a vertical surface is convected downstream, disturbance components amplify selectively and in a very narrow band of frequencies; further downstream, non-linear and three-dimensional effects become important [4]. Key aspects of the transition of an initially stable laminar natural convective flow to turbulence were clarified in refs [5, 6]: the first signs of turbulent disturbances were found to appear in the velocity boundary layer without alteration of the temperature profile from the laminar form until reaching a point, further downstream, where the velocity disturbances become strong enough to change the temperature profile (the onset of thermal transition). The thermal transition region ends with the development of a completely turbulent boundary region where all flow variables fluctuate randomly (fully turbulent region). Despite many research efforts, the pioneering experimental investigations of transitional effects, summarized in refs [4, 6] and obtained with different fluids, heating conditions, surface sizes and instrumentation (hot wire, thermocouples, interferometer), showed large disagreements concerning the characteristics of the beginning of transition adjacent to a vertical surface. Indeed, the assumption of the Grashof number criterion outlined by Bejan and Lage [7] and still assumed in heat transfer books [8] leads to a large spread of the critical values for the transition; a different correlator of the transition region location (beginning and end of the transition region), termed kinetic energy flux parameter, was proposed in [6]: it depends on the ratio between the Grashof number and the local elevation raised to a given exponent. Regardless of the parameter assumed to assess the end of the laminar regime for the buoyant flow, discrepancies among findings by various researchers when air is used as convective fluid

CONTACT Essam Nabil Ahmed  essameldin.abdo@edu.unige.it  DICCA, University of Genoa, via Montallegro 1, Genoa 16145, Italy

 Supplemental data for this article can be accessed online at <https://doi.org/10.1080/08916152.2024.2357175>.

© 2024 Taylor & Francis Group, LLC

may be also ascribed to the confinement configuration surrounding the heated plate, to poorly controlled thermal gradients, or to slight turbulence of air in the laboratory room [9–11].

Despite the abundant literature dealing with the occurrence of transitional effects for a free-convective flow along a vertical wall, few and often contradictory research works have been devoted to the effect of macroscopic roughness elements on heat transfer from a vertical plate [12]. Roughness elements alter the heat transfer from the plate due to the increased surface area, the more efficient redirection of the convective flow (caused by the surface alteration), and the possible premature transition to turbulence (caused by the occurrence of flow separation and instabilities).

The aim of this investigation is twofold. First, observations of the thermal field in a buoyant airflow, induced by a vertical, isothermal, and smooth plate, were performed with focus on conditions close to the end of the laminar regime; second, the effect of the insertion of roughness elements (staggered rows of rib segments of finite length) glued onto the vertical plate was analyzed. The instrumentation employed includes the schlieren optical technique, useful to gain insights into the flow stability and heat transfer coefficient distribution at the wall (only for stable flows), and miniature thermocouples to detect the air temperature fluctuations at several stations in the boundary layer.

Experimental setup and procedure

The test surface was an aluminum plate, 0.5 m high, 0.3 m large, and 0.005 m thick, connected to a plane electrical heater. The plate thickness was enough to ensure that the condition of uniform wall temperature was attained fairly well. The height of the plate was specifically selected to promote, in conjunction with wall-to-air temperature differences of about 50 K, flow conditions not far from the end of the laminar regime (corresponding to a Grashof number of about 10^9 , according to the general consensus [7, 8]). The heater-plate assembly, suspended at about 1.5 m from the floor, was insulated on one side in order to convey as much heat flux as possible toward the side exposed to the ambient air. The plate temperature was evaluated as the average among the readings given by several 0.5 mm-dia thermocouples (calibrated to ± 0.1 K) embedded at different plate elevations through small holes drilled into the material. The ambient air temperature was calculated by averaging the readings of three thermocouples situated below the heated plate or aligned to the leading edge of the plate.

Even though in principle the experiment deals with the free convection from an unbounded vertical surface, the presence of confinement structures of the heated plate is necessary to prevent significant interaction with air movements in the laboratory room. Main body of experiments were performed by using a closed shield, below the heated plate, with openings in its bottom part to permit the buoyant air to enter and flow along the heated plate. To avoid significant sidewise air entrainment and minimize disturbances from the environment, the heated plate was then bounded on both sides by two glasses, 10 cm long and as high as the heated plate and shrouded by a frontal polystyrene wall, placed at a distance from the heated plate (25 cm) equal to half of the plate height. This configuration (A), schematically shown in [Figure 1a](#), is similar to that used in previous literature studies (e.g., refs [13, 14]). A slightly different confinement of the plate (B) is presented in [Figure 1b](#): here the lateral access of ambient air is completely inhibited, and air is constrained to flow only coming from the bottom (while in case A air comes from the bottom and, in part, from the side openings). A third example of confinement (C), similar to that used in experiments by Warner and Arpaci [10] and typically adopted for numerical simulations (e.g., [15]): the approaching flow is completely enclosed in a box (including a horizontal surface at short distance upstream of the leading edge of the heated plate) with ambient air entering the box through side slots and exiting through the top open surface, as shown in [Figure 1c](#). The main difference between configurations A and C is the presence of the horizontal wall that forces the airflow to pass through the side openings, redirect toward the plate, and exit through the open top of the box. A fourth arrangement (D) is depicted in [Figure 1d](#): the frontal polystyrene wall is here placed at 8 cm-distance from the heated plate; as compared to the configuration B, the shorter spacing between the two facing vertical walls (8 cm instead of 25 cm) is likely to induce a channel flow throughout the entire cross-sectional area of the confinement structure.

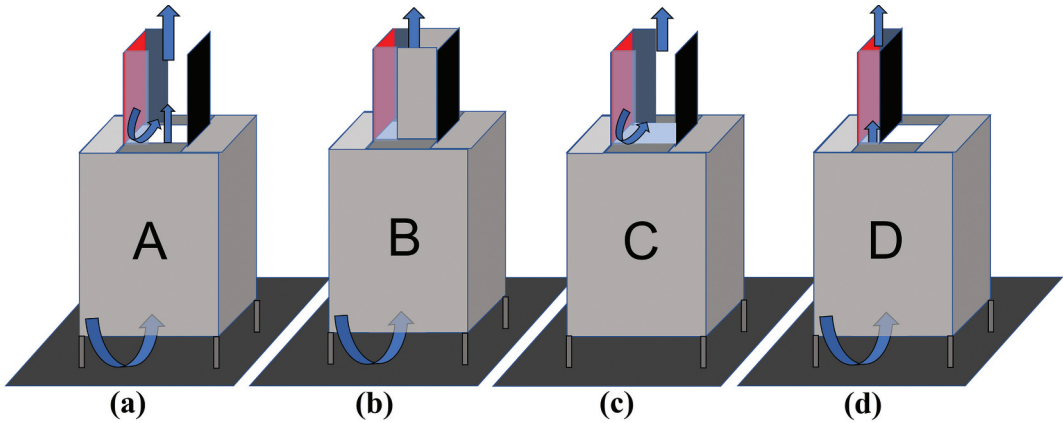


Figure 1. Natural convection experiments and configurations of confinement of the heated vertical plate (colored in red).

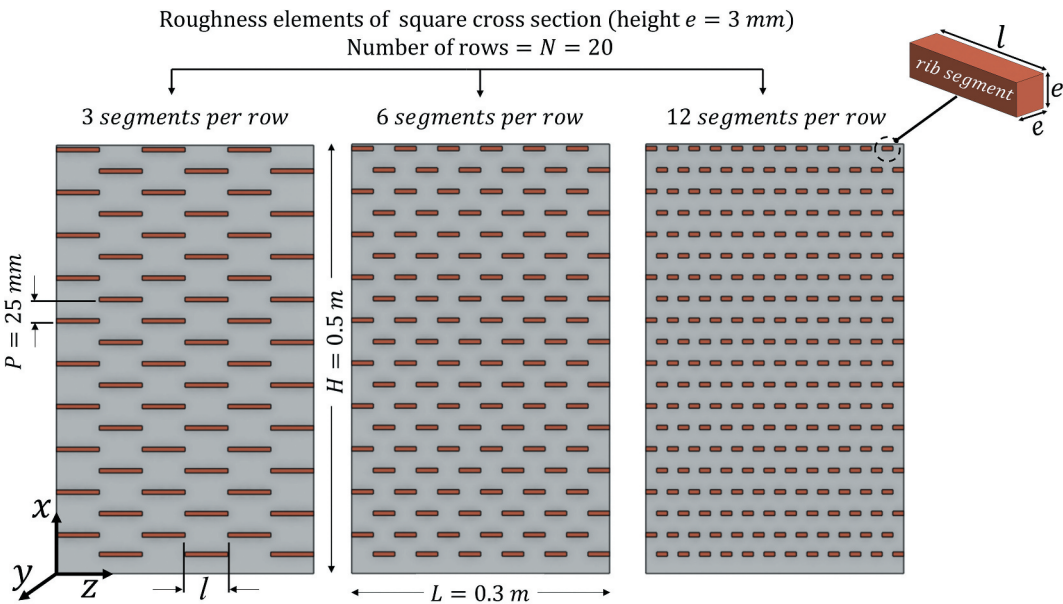


Figure 2. Sketch of the heated plate (frontal view) with roughness elements: segments are square in section with fixed height e , while the segment length l and the corresponding number of segments per row are varied from one experiment to another. H is the vertical plate height, L is the spanwise length of the plate, N is the number of rows, and P is the row pitch.

Table 1. Geometric details of the roughness pattern.

N	e (mm)	P (mm)	l (mm)	segments per row	P/e	e/H	l/L	l/P
20	3	25	50	3	8.33	6×10^{-3}	0.1667	2
20	3	25	25	6	8.33	6×10^{-3}	0.0833	1
20	3	25	12.5	12	8.33	6×10^{-3}	0.0417	0.5

Additional tests were subsequently performed adding macroscopic roughness elements, namely rows of three, six, or twelve rib segments periodically arranged in a staggered pattern. Details of roughness element geometry are reported in [Figure 2](#) and [Table 1](#).

A schlieren optical system was used to visualize the thermal boundary layer and to evaluate the local, natural convective, heat transfer coefficient. An exhaustive description of the schlieren apparatus employed is given in refs [16–18]. Basically, it consists of a white light beam (composed of parallel rays) crossing the test section, a concave mirror (i.e., the schlieren mirror), which focuses the light onto its focal plane (i.e., the cutoff plane), a filter, and a camera to acquire a real image of the test section. As shown in Figure 3, when a focal filament (a thin dark strip) is used as a filter, and no thermal gradients are present in the air crossed by the light beam, all light rays are intercepted by the filter when it is placed on the focus of mirror (and the image formed on the camera will be uniformly dark). When thermal gradients (in the y -direction of Figure 3) are present, individual light rays undergo angular deflections whose extent is related to the magnitude of the gradient; consequently, the corresponding spots appear bright in the camera, permitting a reliable visualization of the thermal boundary layer (more precisely of all air particles with a non-zero thermal gradient). The angular deflection α_y of a given light ray (i.e., passing through a given point of coordinates x, y) can be measured by moving the filter (connected to a micrometer) along the focal plane of the schlieren mirror until the point of interest becomes darkened by the filter. According to this procedure, a single iso-deflection line (line of points inducing the same deflection of light along the y -direction) inside the optical field of view can be visualized. The technique also permits to gain quantitative information: the heat transfer coefficient h can be directly calculated by measuring the deflection of light passing in the vicinity of the wall at the desired location, using the following formula:

$$h = \frac{k(T_w) \alpha_{y,w} T_w^2}{K(T_w - T_{air})}, \quad (1)$$

where T_w and T_{air} are plate wall and ambient air temperatures, respectively, $k(T_w)$ is the air thermal conductivity evaluated at the wall temperature, $\alpha_{y,w}$ is the angular deflection, along the y -direction, of the light ray passing in the vicinity of the wall (i.e., at $y = 0$), and K is a constant ($= 0.024 \text{ m K}$ in the present experiment) which depends on air properties (Gladstone–Dale and ideal gas constants, index of refraction, pressure) and on the length of the plate in the direction of light beam propagation (z -coordinate of Figure 3). Equation (1) assumes the thermal field to be two-dimensional, i.e., independent of z -coordinate; otherwise, it is still valid but the calculated heat transfer coefficient corresponds to the value averaged along the plate length L , that is the plate dimension along the z -coordinate.

The uncertainty in the results (at the 95% confidence level) was evaluated based on the root-sum-square of the individual uncertainties in the measurements of each quantity. The main source of error

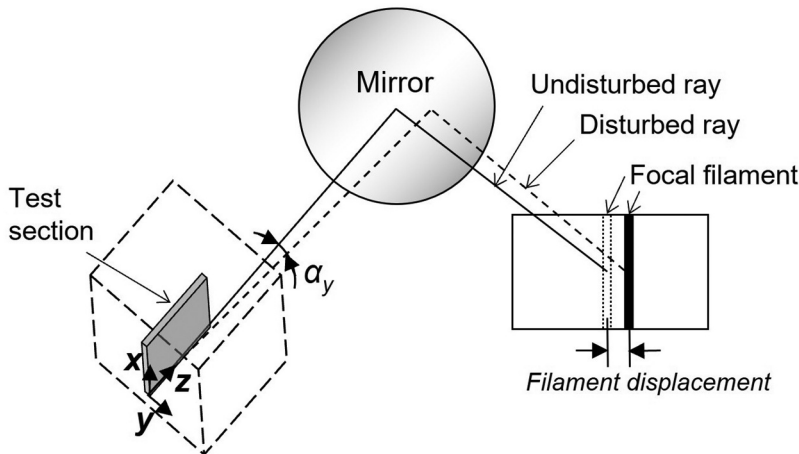


Figure 3. Focal filament schlieren method: the angular deflection of perturbed light rays is detected by shifting the focal filament filter in the focal plane of the schlieren concave mirror.

in the calculation of the local heat transfer coefficient h is attributed to the measurement of angular deflection of light rays, whose accuracy improves as its value increases (i.e., in the presence of large air temperature gradients). For the present experiments, errors in the light ray angular deflection were calculated to be in the range from 9 to 14%, increasing with the reduction of the recorded angular deflection. As errors in the wall-to-fluid temperature difference are also accounted for, the uncertainty in h (and in the Nusselt number) eventually falls into the $\pm 10\text{--}15\%$ range, while the uncertainty in the Rayleigh number is estimated to be $\pm 5\%$ [19].

Schlieren measurements were supplemented by the detection of air temperature fluctuations in the boundary layer by using a miniature thermocouple with an exposed, $100\ \mu\text{m}$ -dia junction, able to travel along the direction normal to the plate surface, at an arbitrary position along the vertical and spanwise coordinates. A National Instrument acquisition unit (NI PXIe-1078 equipped with a NI TB-4353 module) was used to acquire the air temperature measurements at a frequency of 50 Hz.

Tests were carried out by delivering electrical power to the heater through a DC power supply, adjusting the input voltage to achieve a temperature difference between the heated wall and the ambient air of about 50 K. An isothermal boundary condition was established due to the relatively high thickness of the plate and high thermal conductivity of aluminum. The degree of temperature uniformity of the plate was typically within $\pm 3\%$ of the mean wall-to-ambient temperature difference. After the initiation of each test, steady state was achieved in about 6 – 7 hours. At the end of the test, air and wall temperatures were acquired and schlieren measurements were performed. Measurements of air temperature inside the boundary layer were performed for a number of representative tests, over a time period of about 15 minutes, at different distances from the plate surface and locations along the vertical and spanwise directions.

The Rayleigh and Nusselt numbers, based on the plate height H or the local vertical position x , were introduced as follows:

$$Ra = \frac{g\beta(T_w - T_{air})H^3}{\nu\alpha}, \quad (2)$$

$$Nu = \frac{hH}{k}, \quad (3)$$

$$Ra_x = \frac{g\beta(T_w - T_{air})x^3}{\nu\alpha}, \quad (4)$$

$$Nu_x = \frac{hx}{k}, \quad (5)$$

where h is the local heat transfer coefficient, given by eq. (1), g is the gravitational acceleration, and β , α , ν , k denote the coefficient of thermal expansion, the thermal diffusivity, the kinematic viscosity, and the thermal conductivity of air, respectively. Air properties have been evaluated at the film temperature given by $(T_w + T_{air})/2$, except for β , evaluated at the ambient air temperature.

Since the optical field encompassed a circular region having a diameter of about 20 cm, not enough to frame the entire plate, measurements of the angular deflection of light rays (and the related quantities h and Nu_x) and visualization of the thermal boundary layer were limited to the top third of the heated plate, where the values of Ra_x are the largest.

Results and discussion

The smooth plate

Heat transfer results for the smooth heated plate, in terms of the Rayleigh and the Nusselt numbers based on local elevation x , are displayed in [Figure 4a](#), together with the analytical solution by Ostrach

[21] for a vertical isothermal flat plate and air as the convective fluid. Rayleigh number ($= 0.71 \times Grashof\ number$) signaling, for air, the beginning of transition, according to different authors, are superimposed to the plot (solid line [7], dashed line [10], dash-dotted line [20]). Results, plotted for three different configurations of the plate confinement depicted in Figure 1, fall in a region astride the onset of transition. As mentioned before, experimental data were recorded in a region of the plate close to its trailing edge (last third of the plate height) and, there, values of Nu_x largely exceed (by 20 – 30 percent) the theoretical predictions by Ostrach, valid in the laminar regime. Data obtained for configurations A and B were very close to each other while configuration D yielded further increases in local Nusselt number. No schlieren data were recorded for configuration C as the flow close to the wall was highly unstable. Figure 4b shows the dependence of Nu_x on Ra_x (experimentally obtained) for a shorter vertical plate (of height $H = 0.175\ m$) with different confinement modes (same configurations as in Figure 1) and at three wall-to-fluid temperature differences corresponding to values of $Ra \approx 1.9 \times 10^7$, 1.5×10^7 , and 9×10^6 (all well within the laminar regime). Unlike what had been found in the main experiments (Figure 4a) concerning the plate of larger height ($H = 0.5\ m$), the results for the shorter plate (Figure 4b) were unaffected by the confinement arrangement; this was confirmed by schlieren-based observations of the thermal boundary layer over time (not presented here) which revealed that the flow is always stable. Moreover, the results satisfactorily agree with Ostrach's predictions, thus demonstrating the reliability of the experimental technique to capture accurate local heat transfer coefficient values. Even the deviations realized

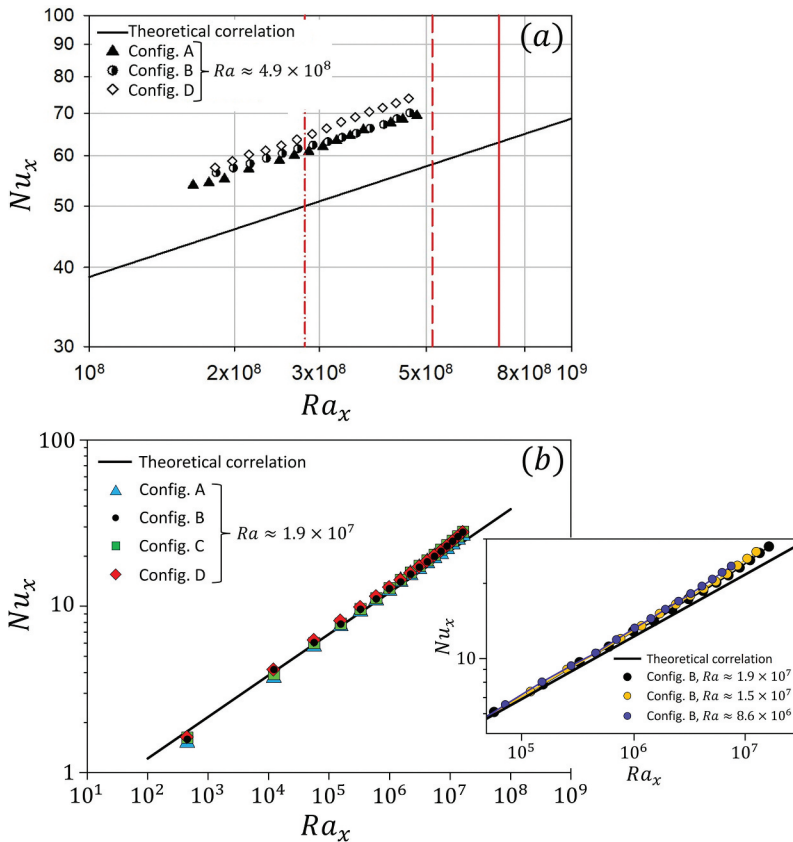


Figure 4. Local Nusselt number versus local Rayleigh number for a smooth, isothermal, vertical plate with different confinement configurations (A, B, C, and D). Results of the main experiments, conducted with the plate of height $H = 0.5\ m$, are plotted in panel (a), with the red solid/dashed/dash-dotted lines indicating the transition onset according to different Authors [7, 10, 20]. Panel (b) is dedicated to the results of additional experiments performed with a shorter plate ($H = 0.175\ m$) to achieve lower values of Ra .

close to the trailing edge of the plate (highlighted in the inset of Figure 4b) are justifiable, since, as pointed out by Ostrach [21] and found by Bhavnani and Bergles [12] in similar experimental circumstances, the slight turbulence in the laboratory room air probably affects the results near the top edge, leading to values in excess by 15% at the most. The effect of these exogenous disturbances is likely to be amplified at larger Ra_x , and the deviations from Ostrach correlation therefore become more pronounced, as seen in Figure 4a.

A possible interpretation of results condensed in Figure 4a can be inferred by schlieren observations (Figure 5) and air temperature measurements over time (Figure 6) in the boundary layer. Figure 5 shows schlieren images of the filament shadow (focal filament set at 0.35 mm from the focus) for the smooth heated plate and different confinements (A, B, C, and D; refer to Figure 1): while for cases A and B the trace is stable (and it reacts to a perturbation damping it until a stable condition is attained), the case C leads to an unstable filament shadow (even in the vicinity of the wall, making unfeasible any heat transfer coefficient measurement) and the case D produces a slightly fluctuating trace, thus explaining the higher heat transfer coefficient recorded, relative to cases A and B; for a better view, the reader is referred to the *Supplemental Video* provided with this article. It is worth noting that, as the recorded schlieren image is a result of an integral of the light angular deflections along a line in the spanwise direction, even a small local instability can be hidden by the integration process and not detected by the schlieren observation. This means that the stability of the trace does not guarantee the absolute laminarity of flow; this is the reason why punctual air temperature measurements are required to provide further information about the stability of the flow.

Inspection of Figure 6 reveals that the air temperature, recorded at an elevation not far from the trailing edge ($x = 0.405$ m, corresponding to $Ra_x = 2.6 \times 10^8$) and at a short distance from the heated plate ($y = 0.005$ m, well inside the boundary layer), is not stable over time but is affected by low-frequency unsteady disturbances which are probably related to uncontrolled air currents in the laboratory room. These instabilities are much more pronounced when the heated plate is confined by a horizontal surface at the leading edge and the sensor is placed close to the plate side edge (case C), but still not related to intrinsic turbulence of the flow as the comparison with air temperature fluctuations recorded, by the same sensor and measurement chain, for a hot forced-air jet induced by a hair dryer seems to suggest. For case C remarkable differences between the time-averaged local temperature in the spanwise direction are also observed, denoting probably marked three-dimensional effect induced by the confinement of the heated plate. Air temperature fluctuations for cases A and

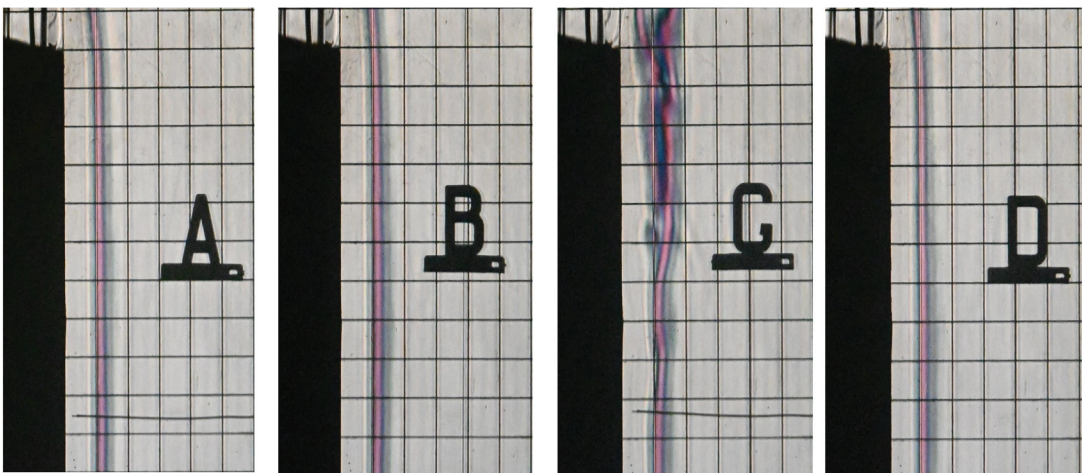


Figure 5. Schlieren images showing the focal filament shadow (focal filament shifted by 0.35 mm from the focus) for the smooth heated plate with different confinement arrangements. A two-dimensional ($x - y$) grid consisting of 1 cm \times 1 cm cells is superimposed; the top 11 cm of the plate are displayed here.

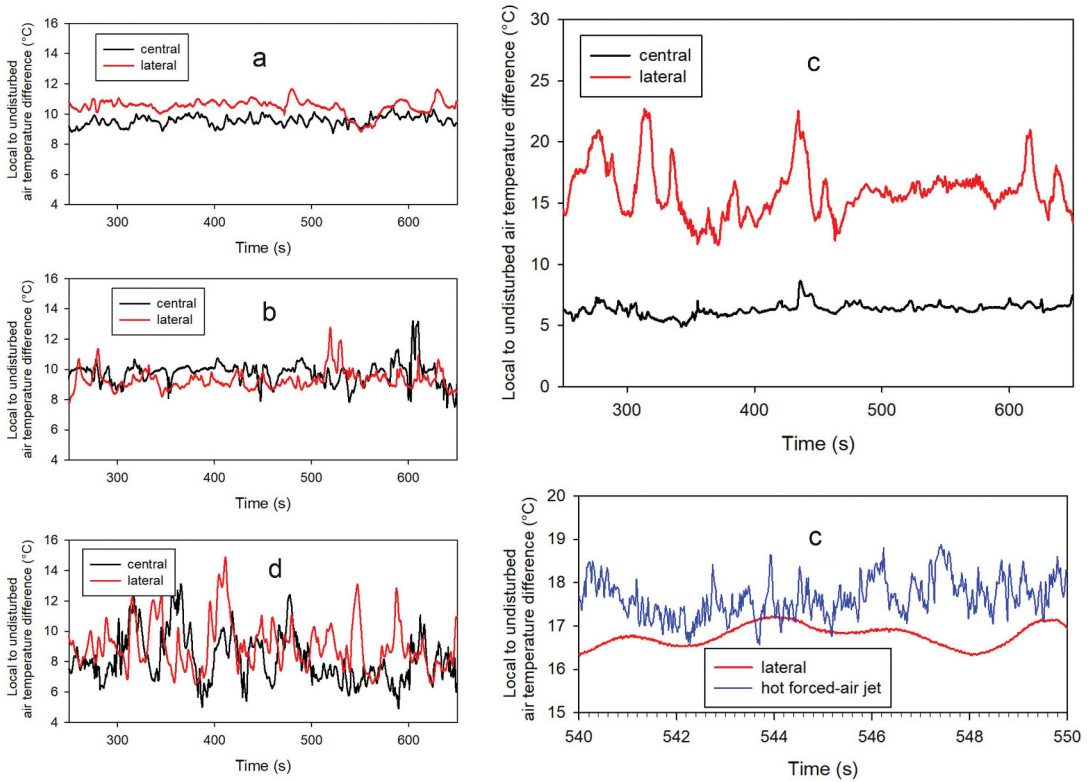


Figure 6. Traces of air temperature fluctuations, recorded at an elevation $x = 0.405$ m ($Ra_x = 2.6 \times 10^8$) and a distance from the heated plate $y = 0.005$ m. With respect to the spanwise coordinate, the sensor was placed at a central or lateral (4 cm from the edge) position. Comparison with fluctuations for a hot forced-air jet (a typical example of turbulence) is shown in the bottom-right frame.

B are qualitatively similar, while for case D, featured by a channel flow, the extent of fluctuations is higher, regardless of the spanwise coordinate. It may be concluded that the flow features, most importantly the recorded low-frequency instability, associated with the particular confinement arrangement adopted are likely to be responsible for the deviation of the local Nusselt number values from those calculated by Ostrach in the laminar flow regime.

The rough plate

The influence of roughening the vertical heated surface is investigated, exploiting the recent findings by the same group of authors [19] together with additional, complementary results and further analysis.

Wooden roughness elements (rib segments having a square section, $e \times e$, and a variable length, l) have been attached to the heated plate (refer to Figure 2) in order to assess their impact on the heat transfer characteristics and the instability of the buoyant airflow. Figure 7 reports the spanwise-averaged Nusselt number recorded only over the last third of the plate (even though the whole heated plate, of height $H = 0.5$ m, was covered with 20 rows of roughness elements). The same wall-to-ambient air temperature difference (50 K) as the smooth plate case was considered, giving $Ra = 4.9 \times 10^8$, while the confinement configuration A of Figure 1 was adopted. The presence of the roughness elements is found to generally increase the heat transfer performance throughout most of the regions between rows of segments, as compared with the smooth plate geometry, if the number of segments per row is properly selected. In fact, an

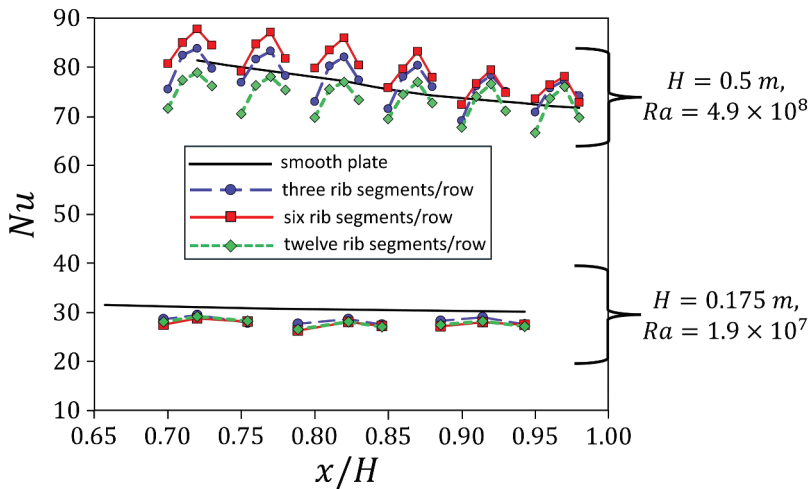


Figure 7. Nusselt number for the smooth and the rough plates: effect of the number of rib segments per row.

optimized number of rib segments per row is likely to exist; within the explored range of parameters, the heat transfer rate from the surface is maximized with six rib segments per row ($l = 25$ mm), which corresponds to a segment length to rib pitch ratio (l/P) equal to 1. It is worth noting that the heat transfer coefficient over the surfaces of the rib segments and the increased surface area (per unit plate height) provided by ribs were not considered in the experimental analysis. Clearly, more pronounced heat transfer enhancements relative to the smooth plate (having the same frontal area) would be observed if the entire roughened surface were considered. Besides, to demonstrate that the effect of perturbing the vertical heated surface is not merely intrinsic to the geometry of the rib segments, but it is also sensitive to the Rayleigh number, the corresponding distributions of Nu when the plate Rayleigh number is decreased by about one order of magnitude (i.e., $Ra = 1.9 \times 10^7$) are plotted in Figure 7. These results are obtained experimentally for a shorter plate ($H = 0.175$ m) roughened with rib segments (again, three, six, or twelve segments/row) having height $e = 2$ mm and pitch $P = 16$ mm, such that the rib pitch-to-height ratio ($P/e = 8$) is close to that for the plate of larger height (for which $P/e = 8.33$, as described in Table 1). It is evident from the figure that no heat transfer enhancement is attainable by roughening the shorter plate and that, at such a low Rayleigh number, the behavior of Nu is almost insensitive to the number of rib segments per row. In the discussions below, we provide insights on the recorded, selective heat transfer augmentation attainable exclusively at relatively large values of Ra , by considering only the plate of $H = 0.5$ m.

Heat transfer coefficient measurements were again supplemented by local air temperature measurements (Figure 8) and schlieren observations of the boundary layer (Figure 9). The sensor for air temperature measurements was placed aligned to a row of rib segments and in the vicinity (within 1 – 2 mm) of the side face of a segment where the instabilities, if any, are likely to be induced. As for the smooth plate, air temperature fluctuations at low frequency were recorded: while for three and twelve rib segments per row the air temperature fluctuations, shown in the left-hand side of Figure 8, were statistically confined within 2% of the wall-to-ambient temperature difference, the temperature fluctuations registered for six segments per row at the same measurement elevation have a significantly larger magnitude. The amplification of disturbances was sensitive to the elevation (i.e., to the local Rayleigh number) as it was not observed close to the leading edge ($x = 0.1$ m). This circumstance is more evident from inspection of the right-hand side of Figure 8, where the distributions of the root-mean-square of the air temperature fluctuations (normalized by the wall-to-ambient temperature difference) along the coordinate normal to the heated plate, are reported for the smooth plate and for

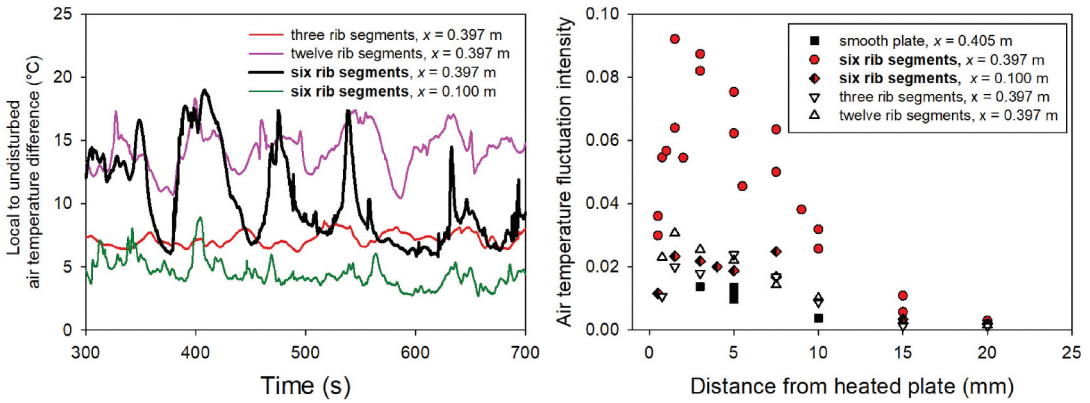


Figure 8. Traces of air temperature fluctuations, recorded at a 5 mm-distance from the plate (in y-direction) and different elevations x , for the rough plate (left) and intensity of air temperature fluctuations as a function of the wall-normal distance, at different elevations x , for the smooth and the rough plate (right).

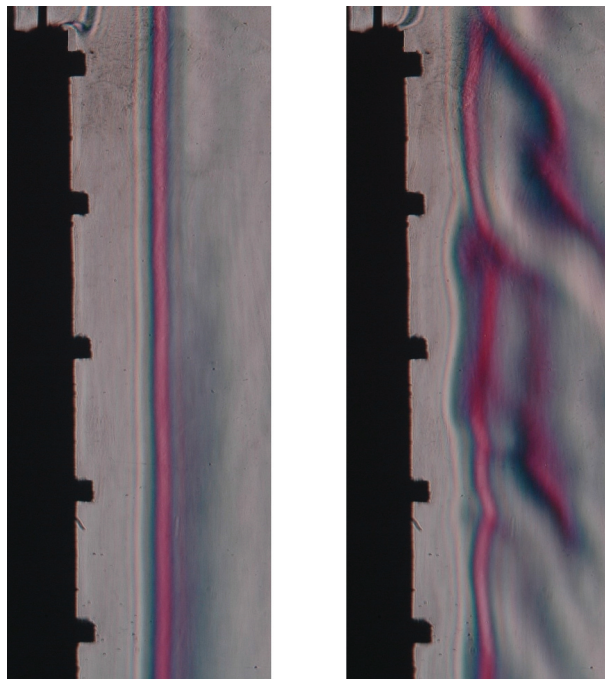


Figure 9. Schlieren images showing the focal filament shadow (focal filament shifted by 0.35 mm from the focus) during low-frequency flow unsteadiness for the rough plate. The pictures refer to the case of six rib segments per row, and the top five rows (out of 20) are framed here.

the rough plate with 3, 6, and 12 rib segments per row. Result shows a peaked profile for the rough plate with six segments per row, at the measurement station close to the trailing edge ($x = 0.397$ m) and in the vicinity of the segment side face, while the rms is markedly lower when detected again in the vicinity of the segment side face but close to the leading edge of the plate ($x = 0.100$ m). Measurements taken for the rough plate with three and twelve rib segments per row, at the same vertical and spanwise coordinates, as well as those obtained for the smooth plate, are featured by markedly lower mean air temperature fluctuations at any distance from the heated plate. Even though the air temperature fluctuation intensity (9% at the most) registered for the rough plate with six

segments per row remains below values that are typically experienced when the transitional and turbulent regimes take place [11], it can be argued that the boundary layer growing along the rough plate with six rib segments per row interacts with, filters and amplifies the exogenous environmental disturbances sufficiently far away from the leading edge of the plate, thus yielding a possible explanation for the larger heat transfer coefficients measured, compared with those recorded for all other geometries explored. Schlieren visualizations (Figure 9) for the rough plate with six rib segments per row provide further evidence of the presence of local unsteadiness: two different schlieren images of the filament shadow (with the focal filament set at 0.35 mm from the focus), taken at different time instants, show that the trace of the filament shadow experiences periodic disturbances at low frequency, with cycles of several seconds (right picture), before recovering a quasi-steady behavior (left picture), thus confirming the evidence of local unsteadiness reflected on the integral optical data recorded by the schlieren setup.

The experimental work was complemented by numerical simulations of the conjugate heat transfer problem, incorporating thermal conduction through the wooden ribs (of thermal conductivity ≈ 0.1 W/m K) and natural convection from the baseplate and the ribs' surfaces to air. The numerical analysis was carried out using Simcenter STAR-CCM +2021.1.1 software (version 16.02.009-R8) and imposing a stable buoyant airflow at the same Rayleigh number of the experiments ($Ra = 4.9 \times 10^8$). The crux here is to investigate whether the staggered arrangement of ribs with six segments per row can still optimize the convective heat transfer rate from the baseplate surface when the effect of flow instabilities/unsteadiness is excluded. Figure 10 shows at a glance the maps of the Nusselt number, Nu , for the rough surface (from left to right: 3, 6, and 12 rib segments per row) over the same plate elevation range ($x = 0.7 H$ to $1.0 H$) explored in the experiments; to facilitate the readability of the figure, only one-third of the plate span (along z -direction) is displayed. The results were analyzed and compared in terms of the spanwise-averaged value of the Nusselt number at each vertical position, x , in a manner similar to that followed in Figure 7: superior heat transfer performance for the rough plate with six segments per row was detected even under stable flow conditions, which implies a better airflow redistribution, relative to the smooth plate case. Nonetheless, the numerical values of the spanwise-

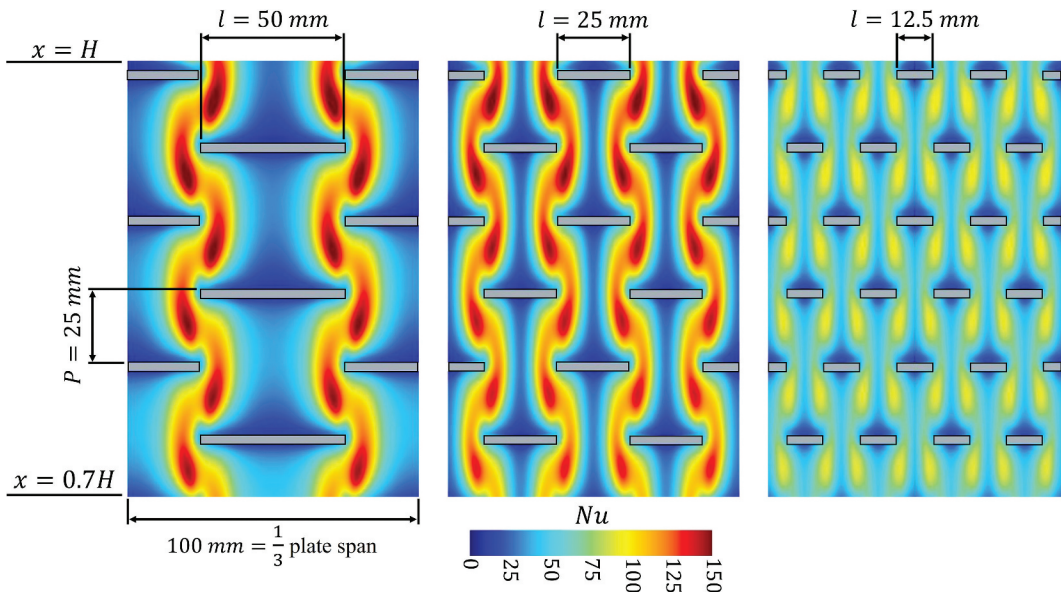


Figure 10. Contours of the Nusselt number, Nu , obtained by numerical simulations in the laminar regime: rib segments having three different lengths (50, 25 and 12.5 mm, corresponding to 3, 6, and 12 segments per row, respectively), $Ra = 4.9 \times 10^8$.

averaged Nu (for the different patterns of ribs and for the smooth surface) are, in general, lower than the experimental values reported in Figure 7. These quantitative deviations are a clear sign of the heat-transfer-promoting effect of the boundary layer instabilities present in laboratory experiments and absent in numerical simulations.

Conclusions

An experimental study on the buoyant airflow along a vertical surface with and without macro-roughness elements has been performed. Attention was directed to the upper part (top third) of the plate; since local conditions were close to transitional, heat transfer measurements were supplemented by local air temperature measurements in the boundary layer to detect possible unsteadiness in the flow, if any.

Main conclusions are summarized as follows:

- (i) natural convection heat transfer results for a smooth, isothermal, vertical plate were found to exceed by 20 – 30% theoretical data from Ostrach, and low-frequency flow instabilities in the boundary layer, sensitive to the different configuration arrangements of the heated plate, were detected;
- (ii) adding roughness elements (rows of discrete rib segments arranged in a staggered pattern) led to an increase of heat transfer coefficient, relative to the smooth plate, especially if a proper size of the segment length is set;
- (iii) analysis of the air temperature fluctuations detected in the boundary layer and close to the segment side face revealed that they are strongly amplified when the optimal number of rib segments per row (six) was selected; these fluctuations are not regarded as intrinsic turbulence but the amplification of exogenous environmental disturbances present in the laboratory room;
- (iv) the heat transfer enhancement provided by the rough plate, with a proper size of rib segments, is likely to be due to the combined effect of the local unsteadiness originating over isolated spots (experimentally observed) and the better redistribution of flow remaining stable elsewhere (numerically deduced).

Disclosure statement

No potential conflict of interest was reported by the authors.

References

- [1] R. P. Dring and B. Gebhart, "A theoretical investigation of disturbance amplification in external laminar natural convection," *J. Fluid. Mech.*, vol. 34, no. 3, pp. 551–564, 1968. DOI: [10.1017/S0022112068002077](https://doi.org/10.1017/S0022112068002077).
- [2] B. Gebhart, "Natural convection flow, instability, and transition," *ASME. J. Heat. Transf.*, vol. 91, no. 3, pp. 293–309, 1969. DOI: [10.1115/1.3580157](https://doi.org/10.1115/1.3580157).
- [3] T. Audunson and B. Gebhart, "Secondary mean motions arising in a buoyancy induced flow," *Int. J. Heat. Mass. Transf.*, vol. 19, no. 7, pp. 737–750, 1976. DOI: [10.1016/0017-9310\(76\)90126-5](https://doi.org/10.1016/0017-9310(76)90126-5).
- [4] R. L. Mahajan and B. Gebhart, "An experimental determination of transition limits in a vertical natural convection flow adjacent to a surface," *J. Fluid. Mech.*, vol. 91, no. 1, pp. 131–154, 1979. DOI: [10.1017/S0022112079000070](https://doi.org/10.1017/S0022112079000070).
- [5] Y. Jaluria and B. Gebhart, "On transition mechanisms in vertical natural convection flow," *J. Fluid. Mech.*, vol. 66, no. 2, pp. 309–337, 1974. DOI: [10.1017/S002211207400022X](https://doi.org/10.1017/S002211207400022X).
- [6] F. Godaux and B. Gebhart, "An experimental study of the transition of natural convection flow adjacent to a vertical surface," *Int. J. Heat. Mass. Transf.*, vol. 17, no. 1, pp. 93–107, 1974. DOI: [10.1016/0017-9310\(74\)90042-8](https://doi.org/10.1016/0017-9310(74)90042-8).
- [7] A. Bejan and J. L. Lage, "The Prandtl number effect on the transition in natural convection along a vertical surface," *ASME. J. Heat. Transf.*, vol. 112, no. 3, pp. 787–790, 1990. DOI: [10.1115/1.2910457](https://doi.org/10.1115/1.2910457).
- [8] A. Bejan, *Heat Transfer*. New York: John Wiley & Sons, Inc, 1993.

- [9] R. Cheesewright, "Turbulent natural convection from a vertical plane surface," *ASME. J. Heat. Transf.*, vol. 90, no. 1, pp. 1–6, 1968. DOI: [10.1115/1.3597453](https://doi.org/10.1115/1.3597453).
- [10] C. Y. Warner and V. S. Arpaci, "An experimental investigation of turbulent natural convection in air at low pressure along a vertical heated flat plate," *Int. J. Heat. Mass. Transf.*, vol. 11, no. 3, pp. 397–406, 1968. DOI: [10.1016/0017-9310\(68\)90084-7](https://doi.org/10.1016/0017-9310(68)90084-7).
- [11] T. Tsuji and Y. Nagano, "Characteristics of a turbulent natural convection boundary layer along a vertical flat plate," *Int. J. Heat. Mass. Transf.*, vol. 31, no. 8, pp. 1723–1734, 1988. DOI: [10.1016/0017-9310\(88\)90284-0](https://doi.org/10.1016/0017-9310(88)90284-0).
- [12] S. H. Bhavnani and A. E. Bergles, "Effect of surface geometry and orientation on laminar natural convection heat transfer from a vertical flat plate with transverse roughness elements," *Int. J. Heat. Mass. Transf.*, vol. 33, no. 5, pp. 965–981, 1990. DOI: [10.1016/0017-9310\(90\)90078-9](https://doi.org/10.1016/0017-9310(90)90078-9).
- [13] G. Tanda, "Natural convection heat transfer from a staggered vertical plate array," *ASME. J. Heat. Transf.*, vol. 115, no. 4, pp. 938–945, 1993. DOI: [10.1115/1.2911390](https://doi.org/10.1115/1.2911390).
- [14] M. Schaub, M. Kriegel, and S. Brandt, "Experimental investigation of heat transfer by unsteady natural convection at a vertical flat plate," *Int. J. Heat. Mass. Transf.*, vol. 136, pp. 1186–1198, 2019. DOI: [10.1016/j.ijheatmasstransfer.2019.03.089](https://doi.org/10.1016/j.ijheatmasstransfer.2019.03.089).
- [15] J. Hærvig and H. Sørensen, "Natural convective flow and heat transfer on unconfined isothermal zigzag-shaped ribbed vertical surfaces," *Int. Commun. Heat. Mass. Transf.*, vol. 119, pp. 104982, 2020. DOI: [10.1016/j.icheatmasstransfer.2020.104982](https://doi.org/10.1016/j.icheatmasstransfer.2020.104982).
- [16] F. Devia, G. Milano, and G. Tanda, "Evaluation of thermal field in buoyancy-induced flows by a schlieren method," *Exp. Therm. Fluid Sci.*, vol. 8, no. 1, pp. 1–9, 1994. DOI: [10.1016/0894-1777\(94\)90067-1](https://doi.org/10.1016/0894-1777(94)90067-1).
- [17] G. Tanda and F. Devia, "Application of a schlieren technique to heat transfer measurements in free-convection," *Exp. Fluids*, vol. 24, no. 4, pp. 285–290, 1998. DOI: [10.1007/s003480050175](https://doi.org/10.1007/s003480050175).
- [18] G. Tanda, M. Fossa, and M. Misale, "Heat transfer measurements in water using a schlieren technique," *Int. J. Heat. Mass. Transf.*, vol. 71, pp. 451–458, 2014. DOI: [10.1016/j.ijheatmasstransfer.2013.12.022](https://doi.org/10.1016/j.ijheatmasstransfer.2013.12.022).
- [19] G. Tanda, E. N. Ahmed, and A. Bottaro, "Natural convection heat transfer from a ribbed vertical plate: Effect of rib size, pitch, and truncation," *Exp. Therm. Fluid Sci.*, vol. 145, pp. 110898, 2023. DOI: [10.1016/j.exptthermflusci.2023.110898](https://doi.org/10.1016/j.exptthermflusci.2023.110898).
- [20] E. R. G. Eckert and E. Soehngen, "Interferometric studies on the stability and transition to turbulence of a free convection boundary layer," *Proc. Gen. Disc. Heat Transf.* 1951, pp. 321–323. London.
- [21] S. Ostrach, "An analysis of laminar free-convection flow and heat transfer about a flat plate parallel to the direction of the generation body force," 1953, NACA Technical Report 1111.